

Screening of Two Sulphur-Containing Schiff's Bases Corrosion Inhibition Properties on CS: Gravimetric, Electrochemical and Quantum Chemical Studies

J. Reeja, K. Joby Thomas*, K. Ragi and M. P. Binsi

*Centre for Electrochemical Studies, Research Division, Department of Chemistry,
St. Thomas' College (Autonomous), Thrissur, Kerala - 68000, India*

*Corresponding author: drjobythomask@gmail.com

Received 08/04/2020; accepted 15/09/2021
<https://doi.org/10.4152/pea.2022400401>

Abstract

Novel sulphur (S)-containing Schiff's bases, N-((1H-indol-3-yl)methylene)thiazol-2-amine (I3A2AT) and (13E)-N1,N2-bis((thiophene-2-yl)methylene) cyclohexane-1,2-diamine (T2CDACH), were synthesized. The structures were deep-rooted by mass, UV-visible, Fourier transform infrared spectroscopy (FTIR) and nuclear magnetic resonance (NMR) analyses. The ligands inhibition efficiency ($\eta_w\%$) on carbon steel (CS) corrosion in 1 M hydrochloric acid (HCl) was studied using gravimetric analysis, electrochemical impedance spectroscopy (EIS), potentiodynamic polarisation (PDP), electrochemical noise (ECN), quantum chemical and surface studies. Both Schiff's bases acted as excellent inhibitors on CS corrosion in 1 M HCl. The excellent inhibitors performance was confirmed by the formation of protective adsorption films onto the CS surface. The inhibitors adsorption onto the CS surface followed Langmuir's adsorption isotherm. Energies of the highest and lowest occupied molecular orbitals (E_{HOMO} and E_{LUMO}), number of electrons transferred (ΔN), electronegativity, chemical hardness, and so forth, were evaluated by quantum chemical studies. An acceptable correlation was observed between the results of quantum chemical calculations and other corrosion monitoring techniques.

Keywords: adsorption, $\eta_w\%$, PDP, quantum chemical approach and S-containing corrosion inhibitors.

Introduction

Iron (Fe) and its alloys are widely used as construction materials in numerous industrial areas, such as petroleum and chemical industries, power plants, etc., due to their high mechanical strength, easy fabrication and low cost [1, 2]. There is a variety of applications that puts steel in contact with assorted corrosive environments, such as acidic solutions, during the processes of acid pickling, descaling and cleaning, etching, oil well acidification, etc. [3]. In acidic media, steel alloys react quickly, and are converted from a metallic to an ionic state, resulting in a vast economic loss. Therefore, there is a vital need to develop some excellent corrosion controlling methods. One of the best way is the use of

corrosion inhibitors [4-6]. They can be classified according to their chemical structure, mode of action, etc. Organic corrosion inhibitors are of the utmost importance, due to their easy synthesis, at relatively low cost, and high protection ability. The corrosion prevention process can be attributed to the inhibitor adsorption onto the steel surface, which hinders the active corrosion sites. The formation of a protective layer on the metal surface delays the metal dissolution, reducing corrosion damage [7, 8]. Many organic molecules possessing aromatic rings and heterocyclic atoms, such as nitrogen (N), oxygen (O), S and phosphorous (P), have proven, practically and theoretically, to be efficient corrosion inhibitors against a wide range of acidic solutions [9, 10], as they play an important role in adsorption centres. In general, the inhibitors having heteroatoms follow the reverse order of their electronegativities, so that, in S, N, O and P, $\eta_w\%$ is in the order of $O < N < S < P$ [11]. The efficiency of these inhibitors can be attributed to their high polarizability and lower electronegativity, so that those atoms and the functional groups can cover large metallic surface areas, which increases the number of electrons transferred (ΔN) to the empty atomic orbital [12]. N-containing organic inhibitors are good anti-corrosion materials for metals in HCl, while compounds with S atoms act as good inhibitors in sulphuric acid (H_2SO_4) [13]. Therefore, in this study, two novel S-containing Schiff's bases were synthesized and selected to act as inhibitors against MS corrosion in a HCl medium.

Materials and methods

Synthesis and characterization

The N-((1H-indol-3-yl)methylene)thiazol-2 amine(I3A2AT) was synthesized by adding a hot ethanol (C_2H_5OH) solution of 2-amino thiazole, in dropwise, to a stirred solution containing an equimolar concentration of indole-3-aldehyde in a C_2H_5OH medium. The mixture was refluxed for 4 h, cooled, and the off-white precipitate was filtered, washed with a C_2H_5OH -water (1:1) mixture, and dried [14]. Its yield was 70% (mp: 168-169 °C).

The heterocyclic (13E)-N1,N2-bis((thiophen-2-yl)methylene)cyclohexane-1,2-diamine (T2CDACH) Schiff's base was synthesized by the condensation of an equimolar mixture of thiophene-2-carbaldehyde and 1,2 diaminocyclohexane, in a C_2H_5OH medium. The reaction mixture was refluxed for 3 h, concentrated and cooled. The cream coloured solid was filtered, washed, and dried. Its yield was 90% (mp: 131 °C). The products were characterized by electronic (Shimadzu UV-visible-1800, dimethyl sulfoxide (DMSO)), mass (Shimadzu, QP 2010 GCMS), NMR (Bruker Advance III HD, deuterated DMSO) and FTIR (Shimadzu Affinity-1, KBr pellet method) spectroscopic analyses.

Gravimetric corrosion inhibition studies

Metal specimen and corrosive medium preparation

CS coupons were cut, abraded with various grades of SiC papers (100, 220, 400, 600, 800, 1000, 1500 and 2000) and washed with distilled water, followed by acetone (C_3H_6O). The approximate composition of the CS specimen was determined by the Energy Dispersive X-Ray Analysis (EDAX)

technique (0.55% C, 0.08% Mn, 0.04% P, 0.012% S, 0.02% Si, and Fe), with a Hitachi SU6600 scanning electron microscope (SEM) model). A stock solution of I3A2AT and T2CDACH (1 mM) was prepared and diluted with a 1 M HCl solution, to obtain different concentrations (0.2-1 mM).

Weight loss (WL) studies.

The metal specimens were immersed in the aggressive medium for 5 days, at 28 ± 0.1 °C, with periodical evaluations of the corrosion rate (CR). The experiments were carried out in duplicate, and the average values were reported. The CR was determined by [15]:

$$v = \frac{K \times W}{D \times S \times t} \quad (1)$$

where $v = CR$ ($\text{mm} \cdot \text{y}^{-1}$), $W =$ weight loss (g), $S =$ surface area of the metal specimen (cm^2), $t =$ time of treatment (h), $D =$ density of the specimen (g/cm^3), and $K =$ constant (8.76×10^4). The $\eta_w\%$ was obtained by the following equation:

$$\eta = \frac{v - v'}{v} \times 100 \quad (2)$$

where v and v' are the metal specimen CR, without and with inhibitor, respectively.

Temperature effect

The temperature effect on the corrosion was evaluated by the WL studies, in the range from 30 to 60 °C. The corrosion activation energy, with and without inhibitors, was calculated by Arrhenius equation [16]:

$$K = A \exp\left(\frac{-E_a}{RT}\right) \quad (3)$$

where K is the CR, E_a is the activation energy, A is the frequency factor, T is the temperature in the Kelvin (K) scale and R is the gas constant. Arrhenius curves were obtained by plotting $\log K$ against $1000/T$. Enthalpy and entropy of activation (ΔH^* and ΔS^*) were calculated from the transition state theory, which can be represented by the following equation:

$$K = \left(\frac{RT}{Nh}\right) \exp\left(\frac{\Delta S^*}{R}\right) \exp\left(\frac{-\Delta H^*}{RT}\right) \quad (4)$$

Electrochemical corrosion studies

Electrochemical studies were made using a three-electrode cell assembly consisting of CS (exposed area of 1 cm^2), platinum (Pt) electrode (1 cm^2) and saturated calomel (SC), as working, counter and reference electrodes (WE, CE and RE), respectively, at 28 °C. For corrosion, the working area of the metal specimens was put in contact with HCl, for 30 min, before the experiment. An Ivium Compact stat-e electrochemical system, with an Iviumsoft software package, was used to perform the experiments.

EIS studies

EIS measurements were taken at a constant potential, in the frequency range from

1 KHz to 100 mHz, with an amplitude of 10 mV as excitation signal [17-19]. The inhibition percentage was calculated by the equation:

$$\eta_{\text{EIS}} \% = \frac{R_{\text{ct}} - R'_{\text{ct}}}{R_{\text{ct}}} \times 100 \quad (5)$$

where R_{ct} and R'_{ct} are the WE charge transfer resistances, with and without inhibitor, respectively.

PDP studies

PDP studies were carried out by changing the WE potential from +250 to -250 mV, with a sweep rate of 1 mV/s [20]. The slope analysis of the Tafel curves gave the corrosion current densities, and the $\eta_{\text{pol}}\%$ was calculated by:

$$\eta_{\text{pol}} \% = \frac{I_{\text{corr}} - I'_{\text{corr}}}{I_{\text{corr}}} \times 100 \quad (6)$$

where I_{corr} and I'_{corr} are the WE (MS exposed area) corrosion current densities without and with inhibitors, respectively.

ECN studies

The experiments were performed in a three-electrode cell assembly, which consisted of two CS (1cm²) and one SC electrodes. All ECN analyses were conducted for a period of 1200 s [21]. An Ivium Compact stat-e electrochemical system controlled by Ivium software was employed for the ECN studies.

Surface morphological studies

SEM images were recorded using a Hitachi SU6600 SEM model, after treatment with a 1 M HCl solution, with and without the inhibitors, for 24 h.

Quantum chemical studies

GAMMES software and the DFT method were used for the determination of the compounds optimized geometry and quantum chemical evaluations. A combination of Lee–Yang–Parr’s nonlocal correlation functional (B3LYP) and Beck’s three parameter exchange functional was employed in the DFT method [22-24].

Results and discussion

The synthesized inhibitor molecules structures were confirmed by spectroscopic techniques.

Molecules structure

I3A2AT analysis calculated for C₁₂H₉N₃S: EIMS, m/z 227 (M⁺), 144 (BP, [C₉H₈N₂]⁺), which was generated by the thiazole part loss; IR, $\gamma_{\text{C}=\text{N}}$ 1627 cm⁻¹, $\gamma_{\text{C}-\text{H}}$ 2930 and 3043cm⁻¹, $\gamma_{\text{N}-\text{H}}$ (br) 3157 cm⁻¹, $\gamma_{\text{C}=\text{C}}$ 1438 cm⁻¹, $\gamma_{\text{C}-\text{N}}$ 1232 cm⁻¹; UV, 29600 cm⁻¹ ($\pi \rightarrow \pi^*$), 25600 cm⁻¹ ($n \rightarrow \pi^*$); ¹HNMR, $\delta_{\text{CH}=\text{N}}$ 7.19(s), δ_{NH} 12.0(d), δ_{CH} in the benzene ring 7.18(t), 7.45(t) δ_{CH} in the thiazole ring 8.01(d),7.43(d), and no inverse peak in DEPT 135 and, hence, the CH₂ group is absent.

T2CDACH analysis calculated for $C_{16}H_{18}N_2S_2$: EIMS, m/z 302 (M^+), 193 (BP, $[C_{16}H_{18}N_2S_2]^+$); IR, $\nu_{C=N}$ 1627 cm^{-1} ; UV, 39525 $cm^{-1}(\pi \rightarrow \pi^*)$, 35971 $cm^{-1}(n \rightarrow \pi^*)$; 1H NMR, $\delta_{CH=N}$ 8.29(s), δ_{CH} in the thiophene ring 7.55(d), 7.30(d), 7.03(t), δ_{CH} in the cyclohexane ring 3.23(t), 1.76(m), 1.40(t), both upward and downward peaks in DEPT 135, due to the presence of CH and CH_2 groups. Fig. 1 shows the I3A2AT and T2CDACH molecular structures and optimised geometries, respectively.

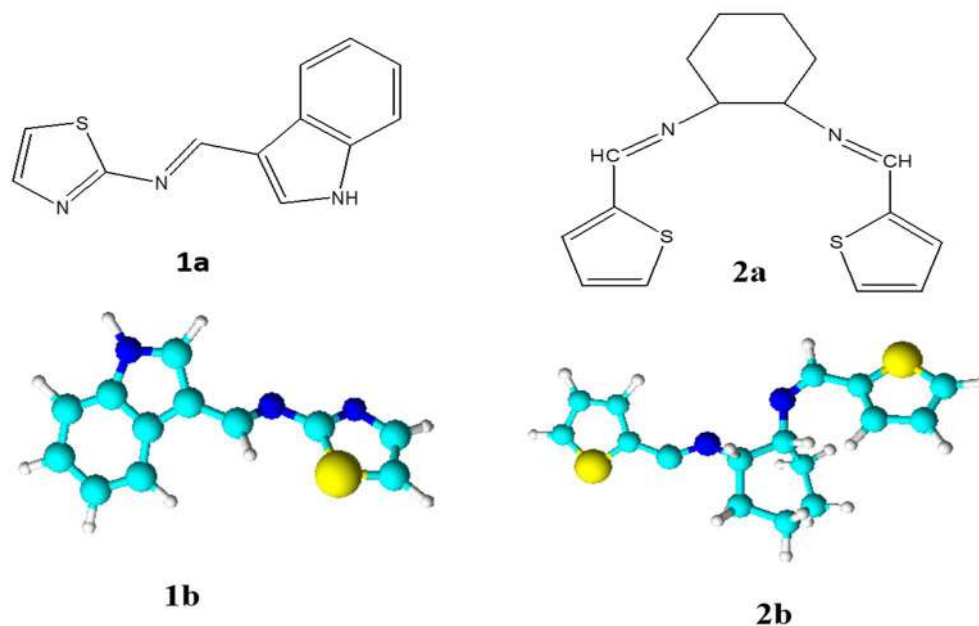


Figure 1. I3A2AT (**1a** and **1b**) and T2CDACH (**2a** and **2b**) Schiff's bases structure and optimized geometries.

Gravimetric corrosion inhibition studies

The I3A2AT and T2CDACH molecules corrosion $\eta_w\%$, for 24 h, at 28 ± 0.1 °C, is listed in Table 1. Both molecules displayed very high $\eta_w\%$ on the CS surface. For a period of 24 h, the I3A2AT molecule showed higher $\eta_w\%$ than that of the T2CDACH molecule, at all concentrations. This may be due to the presence of: an extensively conjugated azomethine linkage; an electron rich aromatic heterocyclic ring containing a highly polarizable S atom; and indole and thiazole moieties. The T2CDACH molecule decreased $\eta_w\%$ may be due to the puckered nature of its aromatic rings.

Table 1. I3A2AT and T2CDACH gravimetric corrosion $\eta_w\%$ on CS in 1 M HCl, for 24 h, at 28 ± 0.1 °C.

Conc. (mM)	I3A2AT	T2CDAH
0.2	91.38	81.42
0.4	93.90	86.59
0.6	94.35	89.83
0.8	94.94	91.15
1	97.61	95.18

Fig. 2 represents the molecules corrosion $\eta_w\%$ variation with time, at 1.0 mM. The plot revealed that the I3A2AT decrease in $\eta_w\%$ was very much steeper than

that of T2CDACH, as the days went on. This may be due to the I3A2AT molecules azomethine linkage (C = N) slow hydrolysis in an acidic medium, which was confirmed by the UV-visible study. The inhibitor stability in the aggressive medium is very important, if it is to be recommended for a prolonged use. From the gravimetric corrosion studies results, one can conclude that the I3A2AT molecule acted as a very good corrosion inhibitor for a long time.

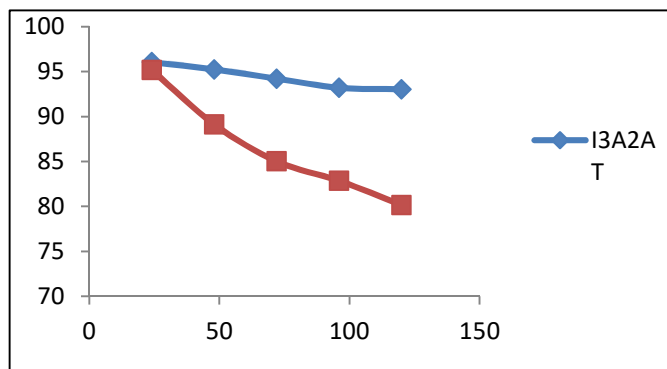


Figure 2. $\eta_w\%$ variation of 1.0 mM I3A2AT and T2CDACH, with time, on CS, in 1 M HCl.

Temperature effect

It is apparent, from the results, that the E_a of the metal dissolution increased with the inhibitor concentration. Table 2 shows the thermodynamic parameters of CS corrosion in 1.0 M HCl, with I3A2AT and T2CDACH. They imply that the metal CR decreased with higher inhibitor concentrations, which can be attributed to the considerable intervention of the ligands during that process.

Table 2. Thermodynamic parameters of CS corrosion in 1.0 M HCl with I3A2AT and T2CDACH.

	Conc. (mM)	E_a	ΔH^*	ΔS^*
I3A2AT	0.2	77.7	55	-34.39
	0.4	112.87	111	143.13
	0.6	114.73	119	148.75
	0.8	120.50	121	160.22
	1	123.44	128	174.47
T2CDAH	0.2	64.04	61.4	-17.64
	0.4	67.64	65	-6.82
	0.6	76.01	73.7	19.59
	0.8	82.58	80	38.74
	1	93.17	90.5	60.18

It is also evident from the thermodynamic data that ΔS^* increased with higher inhibitor concentrations. At the inhibitors low concentrations (0.2 mM I3A2AT, and 0.2 mM and 0.4 mM T2CDAH), ΔS^* exhibited negative values. This suggests that, in the rate-determining step, the activated molecules were in a higher-order state than that at the beginning. As the inhibitors concentration went up, the activated complex disordering increased and ΔS^* attained positive values.

EIS studies

MS corrosion behaviour in 1 M HCl, with and without inhibitor, was examined using EIS, at 28 °C. Figs. 3 and 4 represent CS Nyquist and Bode plots in 1 M HCl, with and without I3A2AT and T2CDACH, respectively.

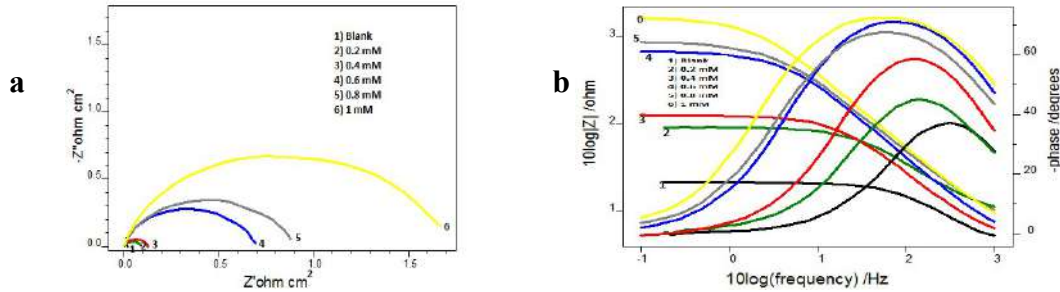


Figure 3. CS a) Nyquist plots and b) Bode plots, with and without I3A2AT in 1 M HCl.

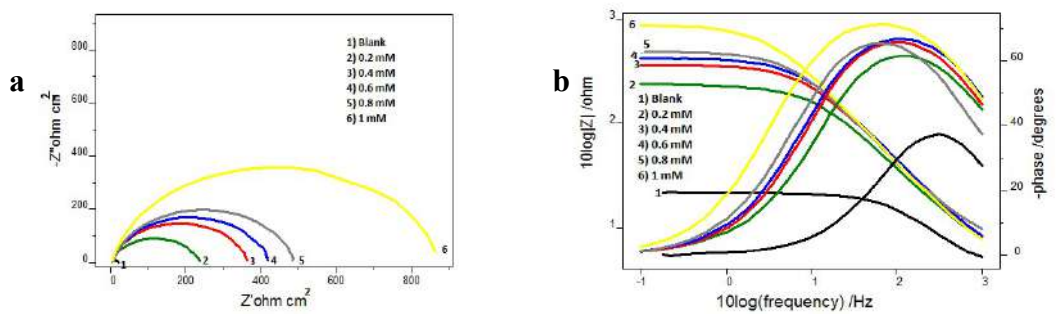


Figure 4. CS a) Nyquist plots and b) Bode plots, with and without T2CDACH in 1 M HCl.

The impedance parameters, including double layer capacitance (C_{dl}), solution resistance (R_s) and $\eta_w\%$, were evaluated from the charge transfer resistance (R_{ct}) values, and are shown in Table 3.

Table 3. Electrochemical impedance parameters of CS corrosion with and without Schiff’s bases, I3A2AT and T2CDACH, in 1 M HCl.

Inhibitors	Conc. (mM)	C_{dl} ($\mu F cm^2$)	R_{ct} (Ωcm^{-2})	η_{EIS} %
Blank	0	101	16.1	-
	0.2	61.4	76.3	78.9
I3A2AT	0.4	76.7	114	85.87
	0.6	57.8	633	97.45
	0.8	57.3	800	97.98
	1	51.5	1540	99.6
	0.2	64.9	211	92.37
T2CDACH	0.4	55.3	334	95.17
	0.6	53.1	386	95.82
	0.8	58.1	449	96.41
	1	59.7	811	98.01

At both high and low frequencies, the capacitance loop intercepted the real axis. These intercepts at the higher-frequency end represent R_s , and, at the lower

frequency end, denote the sum of R_s and R_{ct} . The difference between these intercepts can be calculated to find out R_{ct} , which is the measurement of the electron transfer that takes place on the exposed metallic surface area under analysis, and that is inversely proportional to the surface CR.

The impedance behaviour study was carried out by electric models that helped to evaluate numerical measurements for the chemical and physical properties of the corresponding electrochemical system under investigation. The equivalent circuit that exactly fitted the EIS curves generally consisted of R_s , C_{dl} and R_{ct} (Fig. 5). Table 1 reveals that, with higher inhibitors concentrations of both, R_{ct} values increased and C_{dl} values decreased [25-28].

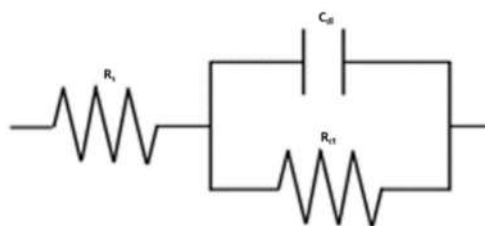


Figure 5. Randles circuit fitted for EIS measurements.

The variation in R_{ct} values can be explained by the adsorption process through which the inhibition mechanism took place. With higher inhibitor concentrations, the adsorption process considerable increased, which prevented the charge transfer of the metal atoms onto the metallic surface and into the solution, resulting in a R_{ct} increase. Lower C_{dl} values with higher inhibitor concentrations can be associated to the local dielectric constant values reduction, and to the rise in the electrical double layer thickness. These observations testify the inhibitor action at the solution-metal interface. From the data, it is obvious that both Schiff's bases, I3A2AT and T2CDACH, acted as potential corrosion inhibitors in HCl.

PDP studies

Tafel extrapolation analysis and linear PDP curves studies (Figs. 6 and 7) were made to establish the impact of the inhibitors on the metal specimens polarization, by the determination of corrosion parameters, such as polarization resistance (R_p), corrosion potential (E_{corr}), corrosion current density (I_{corr}), and $\eta\%$, which are listed in Table 4.

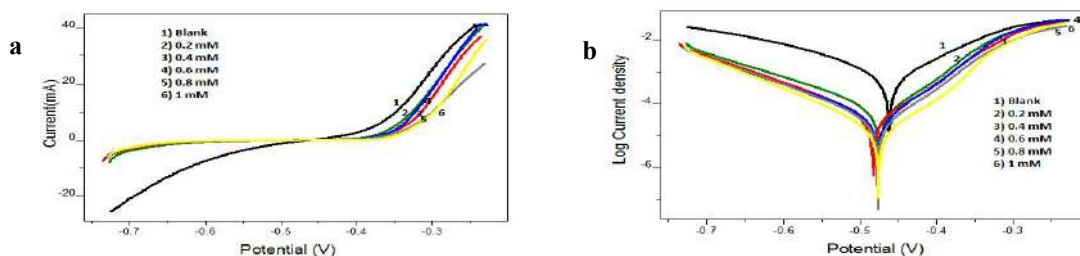


Figure 6. a) Tafel plots and b) Linear PDP curves for MS specimens with and without I3A2AT in 1 M HCl.

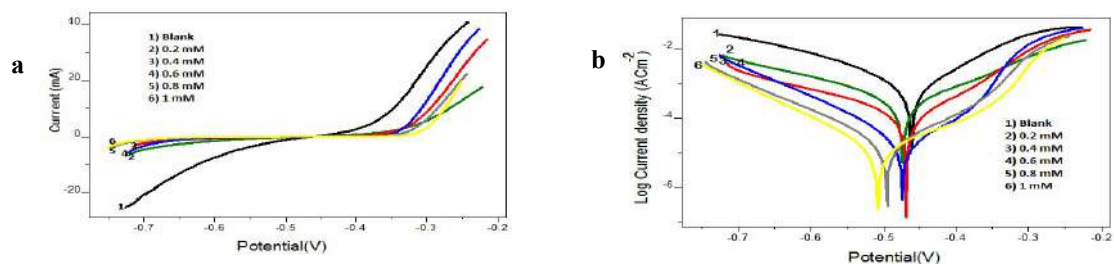


Figure 7. a) Tafel plots and b) Linear PDP curves for CS specimens with and without T2CDACH in 1 M HCl.

Table 4. PPD parameters of CS with and without I3A2AT and T2CDACH in HCl, at 28 °C, for an immersion period of 30 min.

Inhibitors	Conc (mM)	E_{corr} (mV/SCE)	I_{corr} ($\mu\text{A}/\text{cm}^2$)	$-b_c$	b_a	η_{pol} %
I3A2AT	0	-450	1115	110	184	-
	0.2	-473	284	112	208	74.52
	0.4	-467	110	73	205	90.04
	0.6	-474	12.5	43	111	98.86
	0.8	-460	11.1	61	116	98.99
	1	-480	7.6	82	102	99.31
T2CDACH	0	-450	1115	110	184	-
	0.2	-471	77.0	70	134	93.07
	0.4	-468	37.8	63	119	96.60
	0.6	-469	36.0	61	123	96.77
	0.8	-470	30.3	66	115	97.28
	1	-475	12.2	52	103	98.90

Tafel data analysis pointed out that the I_{corr} values significantly decreased, and high $\eta_w\%$ were obtained by both inhibitors in 1.0 mM HCl, even at low concentrations. The maximum $\eta_w\%$ values of 98.15% and 97.83% were shown by I3A2AT and T2CDACH, respectively, at 1 mM concentration in 1 M HCl. This is also congruent with the data obtained in the gravimetric analysis and EIS measurements. In both cases, the cathodic slopes exhibited more predominant changes than the anodic slopes, which is clear evidence for the inhibitors adsorption onto the cathodic sites.

Furthermore, the MS E_{corr} values with I3A2AT and T2CDACH were not significantly altered with respect to those without them. However, an appreciable change was noted in anodic or cathodic slopes in the Schiff's bases, suggesting that, in 1 M HCl, they behaved as mixed-type inhibitors. In other words, the hydrogen evolution process was considerably hindered by both molecules, compared to the Fe oxidation into Fe^{2+} .

ECN studies

ECN experiments were performed with identical CS electrodes and a RE immersed in HCl, with and without I3A2AT and T2CDACH, during 1200 s, at 28 °C.

Fig. 8 represents the current ECN for MS in HCl without and with 1 mM I3A2AT and 1 mM T2CDACH, respectively.

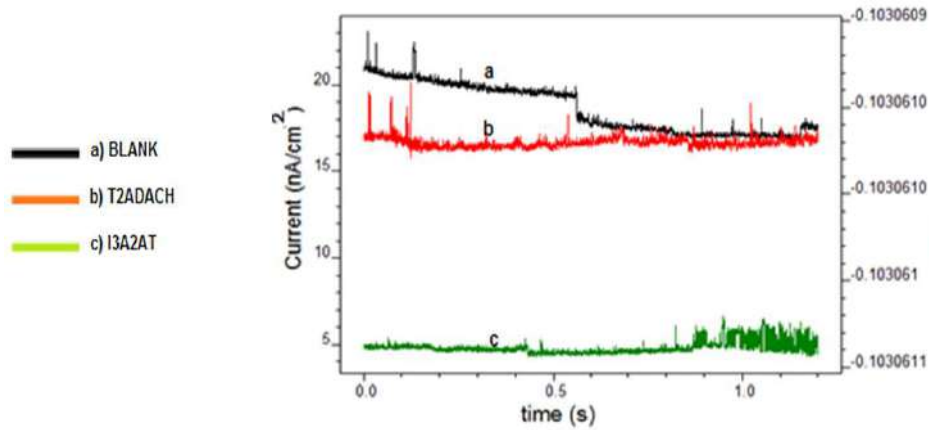


Figure 8. Current ECN for CS with and without I3A2AT and T2CDACH in 1 M HCl, at 28 °C, with 1 mM concentration.

From the ECN data, it is evident that the current ECN mean values followed the order uninhibited solution > I3A2AT > T2CDACH. Potential ECN standard deviation (SD) to current ECN SD gave the ECN resistance (R_{η}) [29]. The inhibited CS R_{η} was much higher than that of the uninhibited metal. The inhibited solutions ECN mean values were lower than those of the uninhibited ones.

The frequency-domain analysis of ECN data gave the power spectral density (PSD) of various systems (Fig. 9).

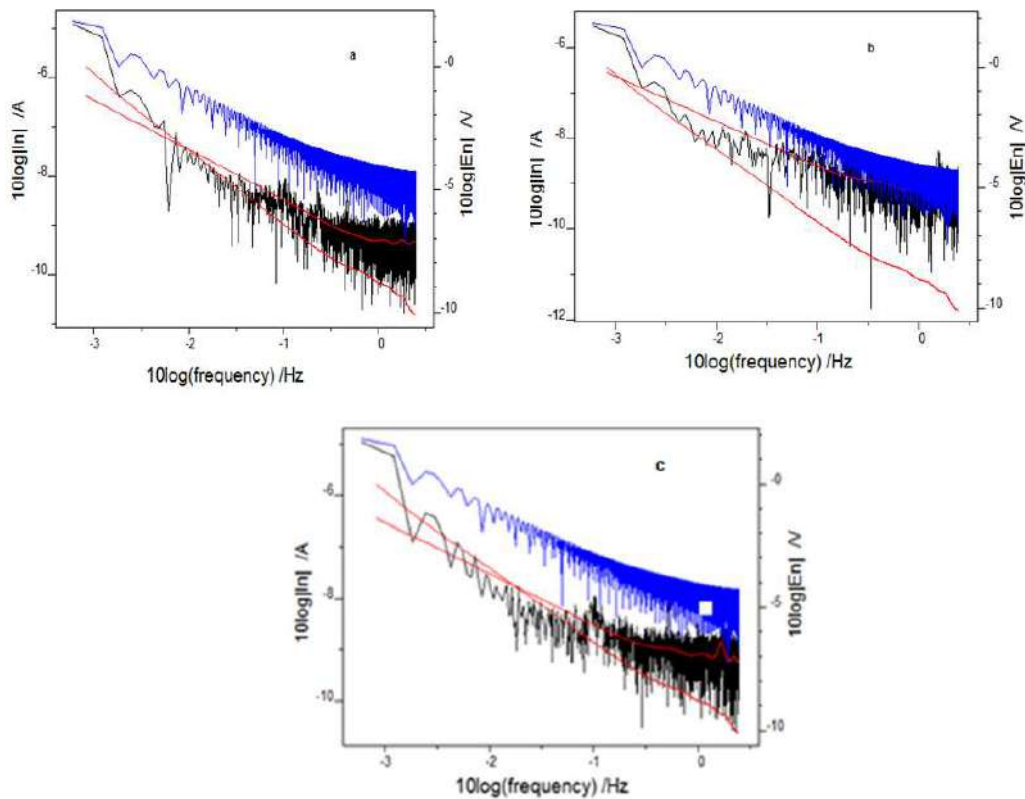


Figure 9. Power spectral density (current and voltage) of CS: (a) without inhibitor; (b) with I3A2AT; and (c) with T2CDACH, in 1 M HCl, at 1 mM concentration.

PSD advantage is that it is independent of time, and its signal statistics do not alter with it [30-32]. Fast FTIR was adopted to convert time-dependent ECN data into PSD plots, using Ivium software. The ECN signals frequency can be monitored with the help of PSD plots. To improve the spectral resolution, Burg introduced a maximum entropy method (MEM) for short time records. Mathematically, this method makes some assumptions about unmeasured data, which are consistent with the existing data. The red lines shown in the fast FTIR spectrum of various CS specimens depict MEM curves.

Current and potential ECN of the uninhibited CS specimen were higher than those of the inhibited specimens. The ECN magnitude was significantly lowered with the frequency. The potential ECN signal higher amplitude indicated appreciable localized metallic corrosion on the uninhibited CS surface [33]. After analysing the PSD plots and MEM curves, it was clear that the potential ECN magnitude values were very much higher for the uninhibited CS specimen than those for the inhibited ones. At all frequencies, potential and current ECN of CS treated with T2CDAC were lower than those of CS treated with I3A2AT, suggesting that the former molecule inhibits relatively well the metal dissolution in 1 M HCl.

The PSD plot slope is an important parameter that depicts the inhibitors molecules response towards the metal surface. A considerable change in the magnitude of a PSD plot slope is a measure of the metal dissolution degree [34, 35]. Though the PSD curves slopes almost remained unchanged for inhibited CS, a significant change in the PSD plots slopes was noticed for the uninhibited metal.

Also, the pitting index values of I3A2AT and T2CDACH were greater than those of the corresponding uninhibited solutions, which indicates resistance to corrosion.

Adsorption studies

The studied Schiff's bases inhibition mechanism can be explained by the adsorption process and resultant surface modifications on the MS surface [35-39]. It can be described by invoking suitable adsorption isotherms, such as Langmuir's, Temkin's, Frumkin's and Freundlich's isotherms.

The adsorption parameters were calculated by selecting the best-fit isotherm model assisted by the correlation coefficient (R²).

Fig. 10 represents the Langmuir's adsorption isotherm for I3A2AT and T2CDACH, in 1 M HCl, which can be expressed as:

$$\frac{c}{\theta} = \frac{1}{K_{ads}} + C \quad (7)$$

where C is the inhibitor concentration, θ is the fractional surface coverage and K_{ads} is the adsorption equilibrium constant value.

The adsorption equilibrium constant, K_{ads} , mainly depends on the standard free energy of adsorption, ΔG^0_{ads} , by the relation:

$$\Delta G^0_{ads} = -RT \ln(55.5 K_{ads}) \quad (8)$$

where 55.5 is the molar concentration of water, R is the ideal gas constant and T is the temperature in Kelvin.

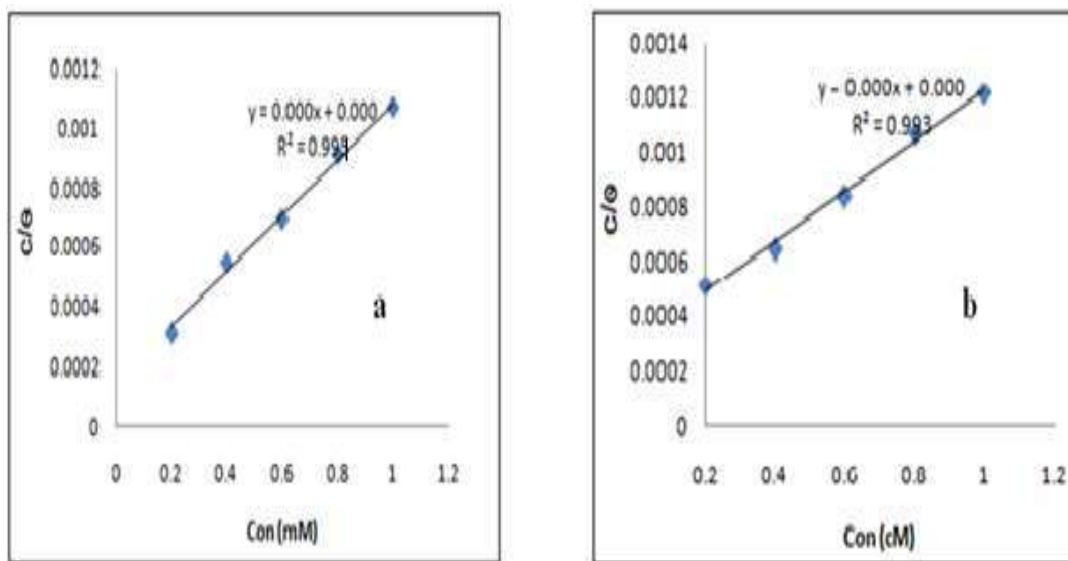


Figure 10. Langmuir’s adsorption isotherms for (a) I3A2AT and (b) T2CDACH, on CS in 1 M HCl.

The derived adsorption parameter values are listed in Table 5.

Table 5. I3A2AT and T2CDACH adsorption parameters, on the CS surface in 1 M HCl.

Thermodynamic parameter	I3A2AT	T2CDACH
K_{ads}	47128.6	33333.3
ΔG^0_{ads} (kJ/mol)	-37.02	-30.37

The adsorption equilibrium constant, K_{ads} , represents the measurement of the adsorption taking place on the corresponding surface. The above data show that I3A2AT has a higher K_{ads} value than that of T2CDACH, which establishes the greater adsorption efficiency of the former. The ΔG^0_{ads} values obtained for I3A2AT and T2CDACH are -37.08 and -30.37 kJ/mol, respectively. The ΔG^0_{ads} values up to -20 kJ mol⁻¹ clearly indicate the electrostatic attraction or physisorption between the charged molecule and the charged metal surface, whereas those lower than -40 kJ mol⁻¹ indicate the inhibitors action on a metallic surface through strong co-ordinate bonds or chemisorption. In the present study, both inhibitors exhibited ΔG^0 values between -20 kJ mol⁻¹ and -40 kJ mol⁻¹, which indicates that the inhibitors absorption behaviour involved chemical and electrostatic interaction.

Surface morphological studies

The MS surface morphology was evaluated with the aid of SEM analysis [40, 41]. Fig. 11(a)-11(d) shows the magnified surface images of MS: bare; immersed in HCl; and immersed in HCl with I3A2AT and T2CDACH (1 M), for 24h.

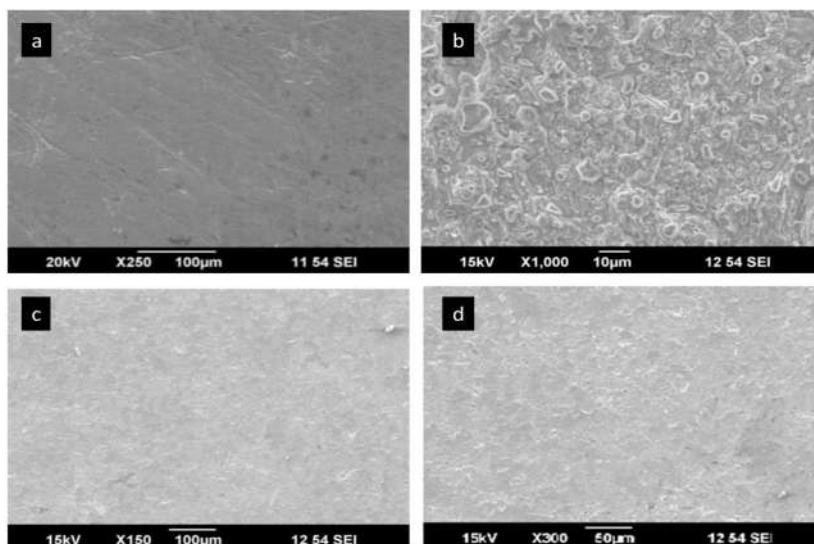


Figure 11. SEM images of CS: (a) bare; (b) in 1 M HCl; (c) in 1 M HCl with I3A2AT (1 mM); and (d) in 1 M HCl with T2CDACH (1 mM), for 24hrs.

The textures of all surface images showed considerable differences. The bare MS pits were due to the polishing effects. The roughness of the MS specimen in HCl was caused by severe corrosion. A smoother MS immersed in HCl with I3A2AT (1mM) and T2CDACH (1mM) resulted from the corrosion prevention by the inhibitors molecules adsorption onto the metal.

Quantum chemical studies

The corrosion inhibition response of organic molecules can be correlated with the frontier molecular orbitals energy. The donor-acceptor interactions (HSAB concept) between the inhibitor molecules filled molecular orbitals and the Fe atoms vacant d-orbitals on the metal surface are very important for the metal dissolution prevention. HOMO gives information on the atomic orbital with the highest contribution and, therefore, about the atom that has the highest tendency to donate electrons. Since it is spread throughout the compound, it is necessary to examine its coefficients, for a better understanding. LUMO is the unoccupied orbital that has the lowest energy, and it indicates the regions in a molecule which have the highest tendency to accept electrons from an electron-rich species.

HOMO energy (E_{HOMO}) provides information about the tendency of a molecule to donate electrons to an electron-poor species. The higher the E_{HOMO} , the greater is the tendency of a molecule to donate its electrons to the electron-poor species. Therefore, a comparison among the E_{HOMO} of the studied compounds indicates the molecules that have the highest tendency to donate electrons to the metal.

The highest and lowest E_{HOMO} values, and the energy difference between HOMO and LUMO (ΔE), are important quantum chemical parameters that facilitate the strong molecule binding on the metal surface. Molecule and quantum chemical calculations geometry optimisation was performed by the DFT method, using GAMMES software. The B3LYP method was employed in DFT calculations [42, 43]. Fig. 12 shows HOMO and LUMO of the studied compounds.

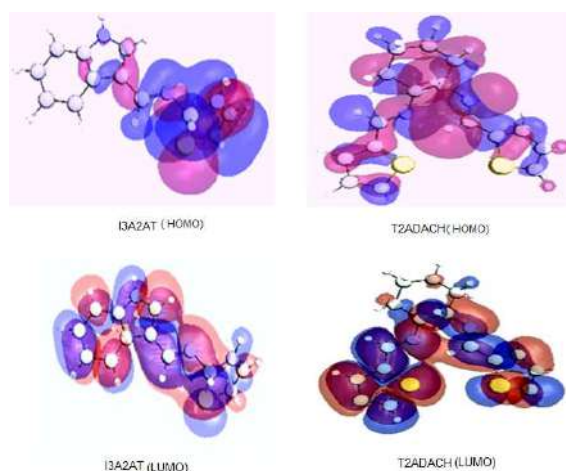


Figure 12. HOMO and LUMO of I3A2AT and T2CDACH.

Table 6 shows the inhibitors quantum chemical parameters which establish that I3A2AT has a higher E_{HOMO} than that of T2CDACH, implying that it has the greater tendency to donate its electrons to the metal surface and, therefore, strongly bind on it. These results are in good agreement with the experimental data.

Table 6. Quantum chemical parameters of I3A2AT and T2CDACH.

Molecule	E_{HOMO} (eV)	E_{LUMO} (eV)	ΔE	I	A	Chemical potential	χ	η	ΔN
I3A2AT	-2.395	1.551	3.946	2.395	-1.551	-0.422	0.422	1.973	1.029
T2CDACH	-3.673	1.016	4.680	3.673	-1.007	-1.333	1.333	2.340	0.672

ΔN indicates the tendency of a molecule to donate electrons. The higher the ΔN value, the greater is the tendency of a molecule to donate electrons to the electron-poor species. In the case of corrosion inhibitors, a higher ΔN implies a greater tendency to interact with the metal surface through the adsorption process. I3A2AT has a higher ΔN value than that of T2CDACH.

According to Lukovits [44, 45], if $\Delta N < 3.6$, $\eta\%$ is increased, with a higher electron-donating ability at the steel surface. In this study, the synthesised inhibitors were the electrons donors, and the MS surface was the electrons acceptor. This result supports the assertion that the inhibitors adsorption onto the MS surface can occur based on donor-acceptor interactions between the compound π electrons and the metal surface vacant d-orbitals.

The dipole moment (μ) is also a significant factor, although there is lack of agreement on the relation between it and the inhibitive performance. Some researchers founded that a low μ value will favour the inhibitor accumulation on the metal surface, increasing its performance [46].

Other researchers suggested that a μ high value, associated to the inhibitor dipole-dipole interaction with the metal surface, can enhance the former adsorption onto the later, and increase its efficiency. In the present work, the I3A2AT μ value was lower than that of T2CDACH, which agrees with the first assumption. According to these inhibitors structures, there are free electron pairs on N and S, which enable to form a σ -bond with Fe. In addition, in HCl case, an electrostatic interaction is possible

between the negatively charge Fe surface, which may be brought about by the Cl⁻ anions specific adsorption, and the positively charged inhibitor. The inhibitors essential effect is due to the presence of free electron pairs in the N and S atoms, p-electrons on the aromatic ring, the type of interaction with the MS surface, and its complexes formation. It is well known that MS has a potential coordination affinity towards N and S donors Schiff's bases. Therefore, the inhibitors adsorption onto the MS surface can be ascribed to the coordination through their heteroatoms and π -electrons of the aromatic rings [47-49]. In the present case, the synthesized inhibitors had unshared electron pairs on N and S, which enabled them to coordinate with MS.

Conclusion

Two novel Schiff's bases, I3A2AT and T2CDACH, are very effective corrosion inhibitors for CS in a HCl medium. $\eta_w\%$ of both ligands has exceeded 95%, which may be due to the highly polarisable S atom, the lone pair of electrons on the N atom, the aromatic rings and the azomethine linkage.

The corrosion monitoring studies revealed that I3A2AT $\eta_w\%$ was greater than that of T2CDACH, at all concentrations. T2CDACH decreased $\eta_w\%$ may be due to the puckered nature of its aromatic ring. Both inhibitors obeyed Langmuir's adsorption isotherm on the CS surface, during the inhibition process. The inhibitors mainly delayed the corrosion process by hindering the cathodic process. The I3A2AT and T2CDACH role in preventing CS localized corrosion in HCl was verified by ECN studies. Quantum chemical studies differentiated the molecules protective power. MS surface analysis by SEM and IR portrayed the inhibitors anticorrosive mechanism.

Acknowledgement

The authors would like to thank the anonymous referees for constructive comments on the earlier version of this paper. The authors are grateful to SAIF-STIC, Cochin University of Science and Technology, for its valuable support.

Authors' contributions

J. Reeja: overall direction, planning and designing of the analysis; carried out synthesis and corrosion inhibition studies; processed the experimental data; performed the analytical calculations and computational studies; wrote the manuscript with input from all authors. **K. Joby Thomas:** conceived and designed the study; analyzed the spectra; edited the manuscript; discussed all results and commented on the manuscript. **K. Ragi:** helped to design the analysis; helped to carried out the analysis work; read and approved the final manuscript; discussed results. **M. P. Binsi:** helped to perform the calculations; did the proof reading; discussed the results and gave critical feedback.

References

1. Verma C, Olasunkanmi LO, Obot IB, et al. 2,4-Diamino-5-(phenylthio)-5H-chromeno [2,3-b] pyridine-3-carbonitriles as green and effective corrosion inhibitors: gravimetric, electrochemical, surface morphology and theoretical studies. RSC Adv. 2016;6(59):53933-48. DOI: <https://doi.org/10.1039/C6RA04900A>

2. Lgaz H, Chung IM, Salghi R, et al. On the understanding of the adsorption of Fenugreek gum on mild steel in an acidic medium: Insights from experimental and computational studies. *Appl Surf Sci.* 2019;463:647-58.
3. Farag AA, Ismail Amr S, Migahed MA. Inhibition of CS corrosion in acidic solution using some newly polyester derivatives. *J Mol Liq.* 2015; 211:915-923. DOI: <https://doi.org/10.1016/j.molliq.2015.08.033>
4. Khadiri A, Saddik R, Bekkouche K, et al. Gravimetric, electrochemical and quantum chemical studies of some pyridazine derivatives as corrosion inhibitors for mild steel in 1 M HCl solution. *J Taiwan Inst Chem Eng.* 2016 1;58:552-64. DOI: <https://doi.org/10.1016/j.jtice.2015.06.031>
5. Khadom AA, Yaro AS, Al Taie AS, et al. Electrochemical, activations and adsorption studies for the corrosion inhibition of low CS in acidic media. *Port Electrochim Acta.* 2009;27(6):699-712. DOI: <https://doi.org/10.4152/pea.200906699>
6. Khadom AA, Rashid K. Adsorption and kinetics behavior of kiwi juice as a friendly corrosion inhibitor of steel in acidic media. *World J Eng.* 2018;15(3):388-401. DOI: <https://doi.org/10.1108/WJE-08-2017-0246>
7. Khadom AA, Musa AY, Kadhum AA, et al. Adsorption kinetics of 4-amino-5-phenyl-4H-1,2,4-triazole-3-thiol on mild steel surface. *Port Electrochim Acta.* 2010;28(4):221-30. DOI: <https://doi.org/10.4152/pea.201004221>
8. Alaneme KK, Daramola YS, Olusegun SJ, et al. Corrosion inhibition and adsorption characteristics of rice husk extracts on mild steel immersed in 1 M H₂SO₄ and HCl solutions. *Int J Electrochem Sci.* 2015;10:3553-67.
9. Noor EA, Al-Moubaraki AH. Thermodynamic study of metal corrosion and inhibitor adsorption processes in mild steel/1-methyl-4[4(-X)-styryl pyridinium iodides/HCl systems. *Mat Chem Phys.* 2008;110(1):145-54. DOI: <https://doi.org/10.1016/j.matchemphys.2008.01.028>
10. Bentiss F, Lebrini M, Lagrenée M. Thermodynamic characterization of metal dissolution and inhibitor adsorption processes in mild steel/2,5-bis(n-thienyl)-1,3,4-thiadiazoles/HCl system. *Corros Sci.* 2005;47(12):2915-31. DOI: <https://doi.org/10.1016/j.corsci.2005.05.034>
11. Popova A, Christov M, Zwetanova A. Effect of the molecular structure on the inhibitor properties of azoles on mild steel corrosion in 1 M HCl. *Corros Sci.* 2007;49(5):2131-43. <https://doi.org/10.1016/j.corsci.2006.10.021>
12. Bhrara K, Kim H, Singh G. Inhibiting effects of butyl triphenyl phosphonium bromide on corrosion of mild steel in 0.5 M sulphuric acid solution and its adsorption characteristics. *Corros Sci.* 2008;50(10):2747-54. DOI: <https://doi.org/10.1016/j.corsci.2008.06.054>
13. Sudheer, Quraishi MA. 2-Amino-3,5-dicarbonitrile-6-thio-pyridines: New and Effective Corrosion Inhibitors for Mild Steel in 1 M HCl. *Ind Eng Chem Res.* 2014;53(8):2851-9. DOI: <https://doi.org/10.1021/ie401633y>
14. Musa AY, Kadhum AA, Mohamad AB, et al. Experimental and theoretical study on the inhibition performance of triazole compounds for mild steel corrosion. *Corros Sci.* 2010;52(10):3331-40. DOI: <https://doi.org/10.1016/j.corsci.2010.06.002>
15. Erdemir S. Synthesis of novel chiral Schiff's base and amino alcohol derivatives of calix[4]arene and chiral recognition properties. *J Mol Struct.* 2012;1007:235-41. DOI: <https://doi.org/10.1016/j.molstruc.2011.10.053>

16. Deng S, Li X, Fu H. Alizarin violet 3B as a novel corrosion inhibitor for steel in HCl, H₂SO₄ solutions. *Corros Sci.* 2011;53(11):3596-602. DOI: <https://doi.org/10.1016/j.corsci.2011.07.002>
17. Niouri W, Zerga B, Sfaira M, et al. Electrochemical and chemical studies of some benzodiazepine molecules as corrosion inhibitors for mild steel in 1 M HCl. *Int J Electrochem Sci.* 2014;9:8283-98.
18. Kuruvilla M, John S, Joseph A. Electroanalytical studies on the interaction of L-serine-based Schiff's base, HHDMP, with copper in sulphuric acid. *J Bio-and Tribo-Corros.* 2016;2(3):19. DOI: <https://doi.org/10.1007/s40735-016-0049-9>
19. Kumari PP, Rao SA, Shetty P. Corrosion inhibition of mild steel in 2 M HCl by a Schiff's base derivative. *Procedia Mat Sci.* 2014;5:499-507. DOI: <https://doi.org/10.1016/j.mspro.2014.07.293>
20. Emregül KC, Atakol O. Corrosion inhibition of iron in 1 M HCl solution with Schiff's base compounds and derivatives. *Mater Chem Phys.* 2004;83(2-3):373-9. DOI: <https://doi.org/10.1016/j.matchemphys.2003.11.008>
21. Bentiss F, Lagrenée M, Traisnel M, et al. Corrosion inhibition of mild steel in 1 M HCl by 2, 5-bis (2-aminophenyl)-1, 3, 4-oxadiazole. *Corrosion.* 1999;55(10):968-76. DOI: <https://doi.org/10.5006/1.3283933>
22. Edward J, Fitelson M. Notes on maximum-entropy processing (Corresp.). *IEEE Transact Inf Theo.* 1973;19(2):232-4. DOI: <https://doi.org/10.1109/TIT.1973.1054965>
23. Jamil DM, Al-Okbi AK, Al-Baghdadi SB, et al. Experimental and theoretical studies of Schiff's bases as corrosion inhibitors. *Chem Centr J.* 2018;12(1):1-9. DOI: <https://doi.org/10.1186/s13065-018-0376-7>
24. Raphael VP, Shanmughan SK, Kakkassery JT. Monitoring the interaction of two heterocyclic compounds on CS by electrochemical polarization, noise, and quantum chemical studies. *Int J Corros.* 2016(3). DOI: <https://doi.org/10.1155/2016/4204532>
25. Gupta NK, Quraishi MA, Verma C, et al. Green Schiff's bases as corrosion inhibitors for mild steel in 1 M HCl solution: experimental and theoretical approach. *RSC Adv.* 2016;6(104):102076-87. DOI: <https://doi.org/10.1039/C6RA22116E>
26. Tang Y, Yang X, Yang W, et al. A preliminary investigation of corrosion inhibition of mild steel in 0.5 M H₂SO₄ by 2-amino-5-(n-pyridyl)-1, 3, 4-thiadiazole: polarization, EIS and molecular dynamics simulations. *Corros Sci.* 2010;52(5):1801-8. DOI: <https://doi.org/10.1016/j.corsci.2010.01.028>
27. Sathiya Priya AR, Muralidharan VS, Subramania A. Development of Novel Acidizing Inhibitors for CS Corrosion in 15% boiling HCl. *Corrosion.* 2008;64(6):541-55. DOI: <https://doi.org/10.1016/j.molliq.2016.03.077>
28. Khan SM, Seikh AH, Baig M, et al. Electrochemical Corrosion Behavior of Spirally-welded API X-70 Line-pipe Steel in Acidic and Salt Media. *Manufact Sci Technol.* 2015;3(5):286-293. DOI: <https://doi.org/10.13189/mst.2015.030515>
29. Verma C, Quraishi MA, Ebenso EE, et al. 3-Amino alkylated indoles as corrosion inhibitors for mild steel in 1 M HCl: Experimental and theoretical studies. *J Molec Liq.* 2016;219:647-60. DOI: <https://doi.org/10.1016/j.molliq.2016.04.024>
30. Elemike EE, Onwudiwe DC, Nwankwo HU, et al. Synthesis, crystal structure, electrochemical and anti-corrosion studies of Schiff's base derived from o-

- toluidine and o-chlorobenzaldehyde. J Molec Struc. 2017;1136:253-62. DOI: <https://doi.org/10.1016/j.molstruc.2017.01.085>
31. Mahjani MG, Sabzali M, Jafarian M, et al. An investigation of the effects of inorganic inhibitors on the CR of aluminum alloy using electrochemical noise measurements and electrochemical impedance spectroscopy. Anti-Corros Meth Mater. 2008;55(4):208-216. DOI: <https://doi.org/10.1108/00035590810887718>
 32. Cottis RA, Loto CA. Electrochemical noise generation during SCC of a high-strength CS. Corrosion. 1990(1):12-9. DOI: <https://doi.org/10.5006/1.3585059>
 33. Bertocci U, Frydman J, Gabrielli C, et al. Analysis of electrochemical noise by power spectral density applied to corrosion studies: Maximum entropy method or fast Fourier transform? J Electrochem Soc. 1998;145(8):2780. DOI: <https://doi.org/10.1149/1.1838714>
 34. Chen C. Nonlinear maximum entropy spectral analysis methods for signal recognition. Electron A Electr Eng Res Stud.1982.
 35. Markhali BP, Naderi R, Mahdavian M, et al. Electrochemical impedance spectroscopy and electrochemical noise measurements as tools to evaluate corrosion inhibition ofazole compounds on stainless steel in acidic media. Corros Sci. 2013;75:269-79. DOI: <https://doi.org/10.1016/j.corosci.2013.06.010>
 36. Mills DJ, Bierwagen GP, Tallman D, et al. Investigation of anticorrosive coatings by the electrochemical noise method. Mater Perform. 1995;34(5).
 37. Cottis RA, Al-Awadhi MA, Al-Mazeedi H, et al. Measures for the detection of localized corrosion with electrochemical noise. Port Electrochim Acta. 2001;46(24-25):3665-74. DOI: [https://doi.org/10.1016/S0013-4686\(01\)00645-4](https://doi.org/10.1016/S0013-4686(01)00645-4)
 38. Hamani H, Douadi T, Daoud D, et al. Corrosion inhibition efficiency and adsorption behavior of azomethine compounds at mild steel/HCl interface. Measurement. 2016;94:837-46. DOI: <https://doi.org/10.1016/j.measurement.2016.09.027>
 39. Ateya BG, El-Anadouli BE, El-Nizamy FM. The adsorption of *thiourea* on mild steel. Corros Sci. 1984;24(6):509-15. DOI: [https://doi.org/10.1016/0010-938X\(84\)90033-7](https://doi.org/10.1016/0010-938X(84)90033-7)
 40. Zhao T, Mu G. The adsorption and corrosion inhibition of anion surfactants on aluminium surface in HCl. Corros Sci. 1999;41(10):1937-44. DOI: [https://doi.org/10.1016/S0010-938X\(99\)00029-3](https://doi.org/10.1016/S0010-938X(99)00029-3)
 41. Soltani N, Salavati H, Rasouli N, et al. Adsorption and corrosion inhibition effect of Schiff's Base ligands on low CS corrosion in HCl solution. Chem Eng Commun. 2016;203(6):840-54. DOI: <https://doi.org/10.1080/00986445.2015.1076801>
 42. Palayoor VR, Kakkassery JT, Kanimangalath SS, et al. Chemical modification at the surface and corrosion inhibition response of two semicarbazones on CS in HCl medium. Int J Industr Chem. 20178(1):49-60. DOI: <https://doi.org/10.1007/s40090-016-0101-0>
 43. Ashassi-Sorkhabi H, Shaabani B, Seifzadeh D. Corrosion inhibition of mild steel by some Schiff's base compounds in HCl. Appl Surf Sci. 2005;239(2):154-64. DOI: <https://doi.org/10.1016/j.apsusc.2004.05.143>
 44. Sastri VS, Perumareddi JR. Molecular orbital theoretical studies of some organic corrosion inhibitors. Corrosion. 1997;53(8):617-22.
 45. Senet P. Chemical hardnesses of atoms and molecules from frontier orbitals. Chem Phys Lett. 1997;275(5-6):527-32. DOI: [https://doi.org/10.1016/S0009-2614\(97\)00799-9](https://doi.org/10.1016/S0009-2614(97)00799-9)
 46. Lukovits I, Kalman E, Zucchi F. Corrosion inhibitors-correlation between

- electronic structure and efficiency. Corrosion. 2001;57(1):3-8. DOI: <https://doi.org/10.5006/1.3290328>
47. Li L, Zhang X, Lei J, et al. Adsorption and corrosion inhibition of *Osmanthus fragran* leaves extract on CS. Corros Sci. 2012;63:82-90. DOI: <https://doi.org/10.1016/j.corsci.2012.05.026>
48. Yüce AO, Mert BD, Kardaş G, et al. Electrochemical and quantum chemical studies of 2-amino-4-methyl-thiazole as corrosion inhibitor for mild steel in HCl solution. Corros Sci. 2014;83:310-6. DOI: <https://doi.org/10.1016/j.corsci.2014.02.029>
49. Zheng X, Zhang S, Li W, et al. Experimental and theoretical studies of two imidazolium-based ionic liquids as inhibitors for mild steel in sulfuric acid solution. Corros Sci. 2015;95:168-79. DOI: <https://doi.org/10.1039/C6RA04900A>